ACS Energy LETTERS

http://pubs.acs.org/journal/aelccp

LETTER

The Crucial Role of Vacancy Concentration in Enabling Superatomic Diffusion in Lithium Intermetallics

Sesha Sai Behara and Anton Van der Ven*

Cite This: *ACS Energy Lett.* 2025, 10, 1772−1778

Read Online

ACCESS | Metrics & More | Article Recommendations | Supporting Information

ABSTRACT: **Anode-free solid-state Li batteries promise significant increases in energy densities compared to current commercial batteries that rely on liquid electrolytes. Major challenges persist in controlling morphological evolution during the plating and stripping of lithium metal at the anode current collector. Elemental additives that alloy with lithium have been found to modify the plating and stripping behavior of lithium. Many alloying elements form intermetallics with lithium and the mobility of Li through these intermetallics is believed to have an important effect on morphological evolution. This study shows that Li transport coefficients through intermetallics span a wide range in values, with the B32 LiAl intermetallic predicted to have a Li tracer diffusion coefficient as high as 10^{-6} cm^2/s at room temperature, which is 8 orders of magnitude larger than that of isostructural B32 LiZn. This work demonstrates the crucial role of vacancy concentration in controlling the mobility of Li atoms through intermetallics. While the migration barriers for Li-vacancy exchanges in both LiAl and LiZn are remarkably low, the superatomic conductivity in LiAl is shown to arise from the unique electronic structure of the B32 LiAl compound, which favors high concentrations of vacancies.**

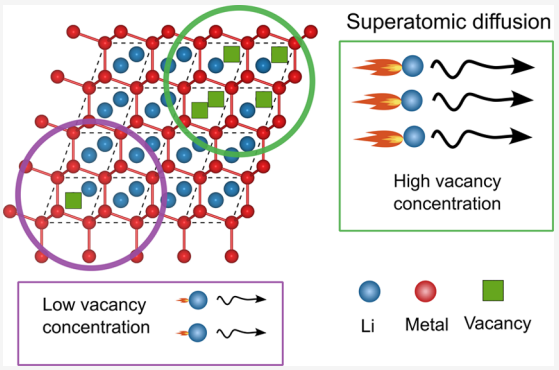

Conventional Li-ion batteries with graphite anodes are fast approaching their theoretical energy density, necessitating an alternative approach to future battery designs.[1] One promising solution is an all-solid-state battery that replaces the graphite anode with lithium metal, thereby enabling a significant increase in the theoretical energy density.[2] However, there are major challenges that restrict the performance of all-solid-state batteries and pose critical safety concerns. One significant impediment is the undesirable morphological evolution of lithium metal upon rapid cycling of the battery. The stripping and plating of lithium metal that occurs at the anode during cycling is known to form voids and dendrites.[3,4] Dendrites can penetrate the solid electrolyte, causing an electrical short circuit, while voids can lead to dead lithium, resulting in loss of contact with the current collector or the electrolyte.[5−7]

The addition of alloying elements or intermetallic interphase layers between the anode current collector and solid electrolyte has been shown to regulate the plating and stripping behavior of lithium metal and increase the cycling capacity of all-solid-state batteries.[8] Multiple alloy systems, including Li−Al, Li−Zn, Li−Ag, Li−Mg and Li−In, have been explored as interphase layers.[9−15] Cao et al.[10] demonstrated that the addition of Zn at the anode improves the ability of lithium metal to wet the solid electrolyte and regulates homogeneous Li deposition. Liu et al.[9] proposed an Al−In alloy-based anode, which showed enhanced cycling capacity at high current densities. Other strategies relying on a thin Mg interlayer or a Ag-carbon composite between the anode current collector and solid electrolyte have also been shown to improve the uniformity of lithium plating and stripping.[11,13,16]

While the underlying mechanisms with which alloying elements improve the plating and stripping behavior of lithium metal remain unclear, their ability to affect the diffusion coefficients of lithium is widely viewed as essential. The low diffusion coefficient of pure Li-metal (~1.6×10^{-10} cm^2/s at room temperature)[17] has been hypothesized as one of the primary reasons for the formation of voids during rapid cycling.[4] Multiple alloying elements have been explored in an

Received: January 23, 2025
Revised: March 5, 2025
Accepted: March 12, 2025
Published: March 18, 2025

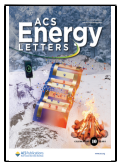

effort to alter the lithium diffusion coefficient.[18−20] While alloying elements such as Mg reduce the lithium diffusion coefficient,[16,17,21] Al and In form intermetallic compounds with Li that exhibit very high lithium diffusion coefficients of ∼10^{-6} cm^2/s at room temperature.[22−24] In fact, the reversibility of the Al−In alloy anode proposed by Liu et al.[9] has been attributed to the high Li diffusion coefficient in the B32-LiAl and LiIn (zintl) phases.

Atom transport in metal alloys and intermetallic compounds occurs primarily through nearest-neighbor atom-vacancy exchanges,[25,26] although second nearest neighbor and multiatom hops can also occur in BCC-based compounds.[27−29] The migration barriers for atom-vacancy exchanges in metal alloys tend to be high due to their compact crystal structures,[28,30,31] limiting atom mobility at room temperature when compared to the mobility of Li in intercalation compounds.[32] Lithium alloys, however, are very different from typical metal alloys.[21,29,33,34] The migration barriers for lithium-vacancy exchanges of some BCC based alloys and intermetallic compounds are predicted to be exceedingly low, ranging between 50 and 150 meV.[21,29,34−38] These barriers are below those of the best superion conducting solid electrolytes.[39−41] Low migration barriers in alloys and intermetallics, however, do not necessarily translate into high atom mobilities, since an atomic hop event can only occur if the atom is next to a vacancy. In most metallic alloys, the concentration of diffusion mediating vacancies is negligible, often being entropically generated due to positive vacancy formation energies.

In this Letter, we demonstrate the crucial role that vacancy concentration plays in enabling Li transport through intermetallic compounds. Using first-principles statistical mechanics techniques, we predict that lithium intermetallic compounds can exhibit superatom transport provided that the electronic and thermodynamic properties of the compound stabilize structural vacancies. We focus on the B32 LiAl and LiZn intermetallics, which have the same zintl crystal structure but very different electronic structures. We find that while the migration barriers for Li-vacancy exchanges in LiAl and LiZn are very low, the unique electronic structure of LiAl leads to high concentrations of structural vacancies that enable superatom transport, with predictions of room temperature tracer diffusion coefficients of 10^{-6} cm^2/s.

Figure 1a shows the crystal structure of B32, which consists of two identical interpenetrating Li and metal networks, each forming a diamond crystal structure. Every lithium (and metal) atom in the crystal structure is tetrahedrally coordinated by four other lithium and metal atoms making up its nearest neighbor shell. The Li sublattices of B32 LiAl and LiZn are fully interconnected by nearest neighbor hops. A vacancy on the Li sublattice can therefore migrate through the crystal without creating antisite defects and thereby disturbing the thermodynamically favored long-range order among Li and the metal of the B32 crystal structure. Examples of nearest neighbor hops on the Li and metal sublattices of B32 are shown in Figure 1a.

First-principles density functional theory (DFT), performed with the Vienna ab initio Simulation package (VASP)[42−44] in combination with the nudged elastic band method as implemented in Transition State Theory Tools for VASP,[45−47] was used to calculate the migration barriers for nearest neighbor Li-vacancy and metal-vacancy hops. Details about the calculations are provided in the Supporting Information. The migration barrier for a nearest-neighbor lithium-vacancy exchange (blue lines in Figure 1b) in both B32 LiAl and LiZn is very low, being less than 100 meV. In fact, the lithium migration barrier in B32 LiZn is approximately 50 meV lower than the barrier in B32 LiAl. These migration barriers are unusually low and are comparable to superion conductors[39−41] and very different than the migration barriers that typify substitutional diffusion in metallic alloys and intermetallic compounds.[30,31,48,49] The migration barriers for metal (Al, Zn) hops in B32 LiAl and LiZn are much higher (red lines in Figure 1b), having a value of 0.65 eV in LiAl and of 0.8 eV in LiZn. These results suggest that lithium can be very mobile in B32 intermetallic compounds, whereas the metal is essentially immobile at room temperature, forming a rigid sublattice.

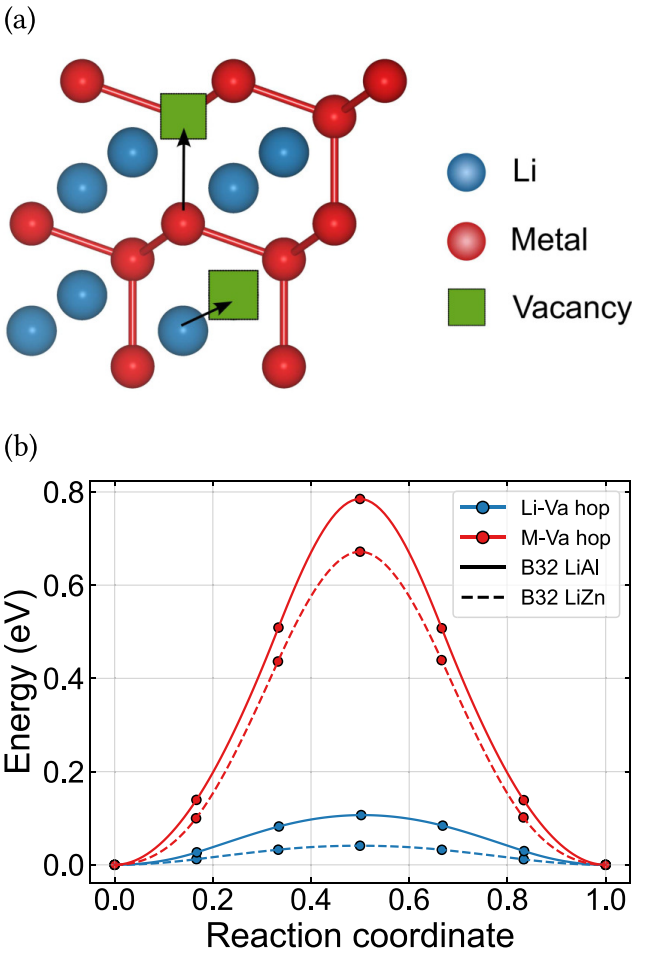

Figure 1. (a) Schematic of Li/metal hopping to a nearest neighbor vacant site in the B32 crystal structure. (b) Migration barriers for Li (metal) hopping to a nearest neighbor vacant site on the Li (metal) sublattice in the B32 crystal structure. The solid (dashed) lines indicate the migration barriers in B32 LiAl (LiZn).

The diffusion coefficients of an intermetallic compound depend not only on the migration barriers for atomic hops *but* also on the availability of vacancies. To determine the vacancy concentrations in the B32 LiAl and LiZn compounds, we calculated the formation energies of a large number of supercells of the B32 structure containing different concentrations of vacancies and antisite defects. The different configurations of vacancy and antisite defects were enumerated with the CASM software package[50] and their formation energies were calculated with DFT using VASP. Figures 2a and

https://doi.org/10.1021/acsenergylett.5c00266
ACS Energy Lett. 2025, 10, 1772−1778

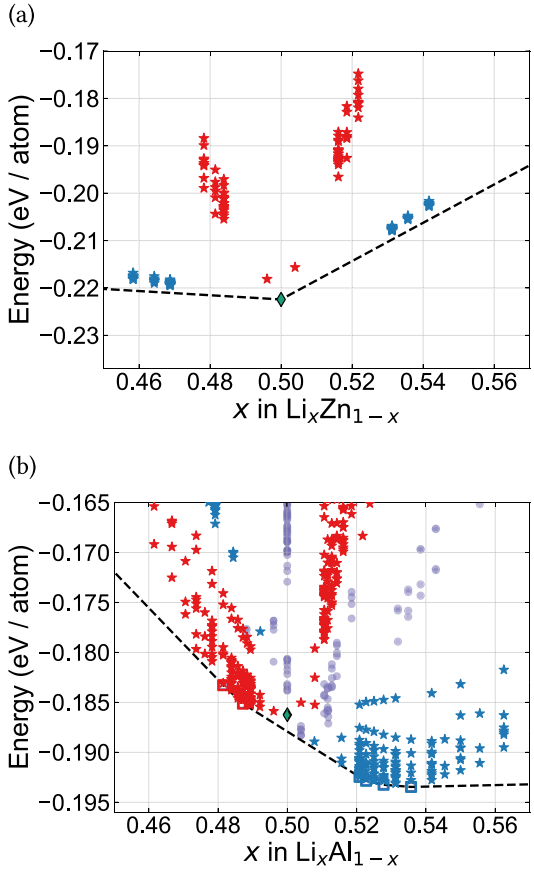

Figure 2. Formation energies of (a) Li−Zn and (b) Li−Al binary systems along with the thermodynamic convex hull. Red (blue) stars indicate structures with *only* vacancies (antisites) defects in the zintl phase. Purple dots indicate structures containing both vacancies and antisite defects. The green diamond shows the formation energy of the perfect B32 crystal structure without any defects. The red (blue) open squares on the Li−Al convex hull (black dashed line in panel (b)) represent stable structures at 0 K containing only Li-vacancies (Li-antisite defects) on the Li (Al) sublattice of B32 LiAl.

2b show the formation energies and convex hulls at 0 K (calculated using DFT) in the vicinity of $x \approx 0.5$ where the zintl phase is stable. The convex hulls were determined using the formation energies of experimentally known intermetallic compounds in the Li−Al and Li−Zn systems. If a structure resides on the convex hull, it is predicted to be stable at 0 K.

In the Li−Zn binary system, the perfect B32 crystal structure (indicated by green diamond in Figure 2a) resides on the convex hull and is therefore predicted to be stable. This is not surprising given that B32 LiZn is an experimentally observed phase in the Li−Zn binary system.[51] The structures containing vacancies (antisites), shown by red (blue) stars in Figure 2a, are above the convex hull and hence not stable at 0 K. However, dilute concentrations of defects can be present in the compound at finite temperatures because of thermal excitations. A rigorous statistical mechanics treatment of defects is necessary in order to calculate their concentrations.[52] However, when defect formation energies are large, their equilibrium concentrations can be approximated by $e^{-\Delta\Omega/k_BT}$, where $\Delta\Omega$ is the vacancy formation energy at constant chemical potential (i.e., within the Grand Canonical ensemble),[34] k_B is the Boltzmann constant, and T is the temperature. Since the calculated vacancy formation energy on the Li sublattice in B32 LiZn ranges between 0.59 eV and 0.68 eV in the voltage window where the B32 phase is stable, the corresponding vacancy concentration ranges between 10^{-12} and 10^{-10} (Figure S3). The vacancy concentration on the Li sublattice of B32-LiZn is, therefore, very dilute, being similar to the predicted vacancy concentration in the pure Li metal.[34,36,53] Note that structures containing antisite defects in Figure 2a are much closer to the convex hull, and a non-negligible concentration of antisite defects can be present at room temperature[54] (Figure S3).

The formation energies of vacancy and antisite defects in the Li−Al system are very different from those of the Li−Zn system. In the Li−Al system, the perfect B32 crystal structure (green diamond in Figure 2b) does not reside on the convex hull. Instead, structures containing lithium vacancies for $x < 0.5$ (red squares in Figure 2b) and lithium antisites (blue squares in Figure 2b) on the Al sublattice for $x > 0.5$ are on the convex hull and are, therefore, predicted to be stable at 0 K. Figure 2b shows that, as the lithium content in the alloy increases, the Li-vacancy (Li-antisites on the Al sublattice) concentration decreases (increases). As opposed to the LiZn zintl phase where the vacancies are *dilute*, and are only *entropically* stabilized at finite temperatures, the vacancies in the LiAl zintl are *abundant*, and are *structurally* stable, even at 0 K.

The high concentration of Li vacancies in the LiAl zintl phase as predicted by DFT has significant implications for Li diffusion. At finite temperatures, thermal excitations will generate disorder among the nondilute concentrations of vacancies on the Li sublattice and Li antisite defects on the Al sublattice. To account for the role of varying degrees of order among the various defects on transport coefficients, we parametrized a coupled sublattice cluster expansion for the B32 crystal structure that accounts for vacancies (antisites) on the Li (Al) sublattice. The cluster expansion was subsequently implemented in Grand-Canonical Monte Carlo simulations to calculate the equilibrium vacancy and antisite concentrations as well as other thermodynamic properties such as the open circuit voltage curve.[31,52,55]

Figure 3a shows the calculated voltage profile (relative to a lithium metal reference anode) at room temperature between $x = 0.46$ and $x = 0.6$ in the Li$_x$Al$_{1-x}$ system. Intermetallic compounds tend to exhibit a sharp step in the voltage profile at their stoichiometric compositions.[29,55] However, the LiAl zintl phase (near $x = 0.5$ in Figure 3a) shows a sloping voltage profile, as a result of the high concentration of vacancies on the Li sublattice and Li-antisite defects on the Al sublattice. The sloping voltage profile also indicates that vacancies are disordered, and are accessible only between ∼0.15 V and 0.38 V. The voltage profile is consistent with the experimental voltage curve measured at 690 K by Wen et al.[24] Figure 3b shows that the vacancy (Li-antisite) concentration decreases (increases) as the Li content in the alloy increases. The predicted defect concentration at room temperature in the LiAl zintl phase is much higher than what is usually observed in metallic alloys or intermetallic compounds. The Li-vacancy concentration is approximately 7 orders of magnitude higher than what is predicted in the LiZn zintl phase and other Li-alloys such as Li−Mg[21] at room temperature.

We next investigated Li diffusion over the Li sublattice of the LiAl zintl phase at room temperature with kinetic Monte Carlo simulations.[57] These simulations rely on cluster expansions to evaluate the energy of the migration barrier and the end states

https://doi.org/10.1021/acsenergylett.5c00266
ACS Energy Lett. 2025, 10, 1772−1778

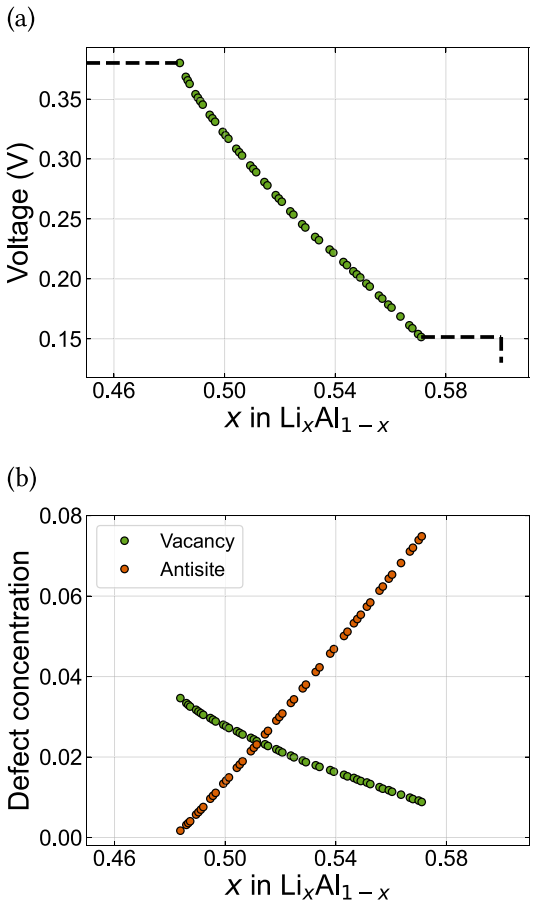

Figure 3. (a) Voltage profile of the LiAl zintl phase at 300 K. (b) Equilibrium vacancy concentration (N_{Va}/N) along with the antisite concentration ($N_{Li\text{-}antisites}/N$) in the LiAl zintl phase at 300 K. N_{Va}, $N_{Li\text{-}antisites}$, and N indicate the number of vacancies, the number of Li-antisites on the Al-sublattice, and the total number of sites in the crystal structure, respectively.

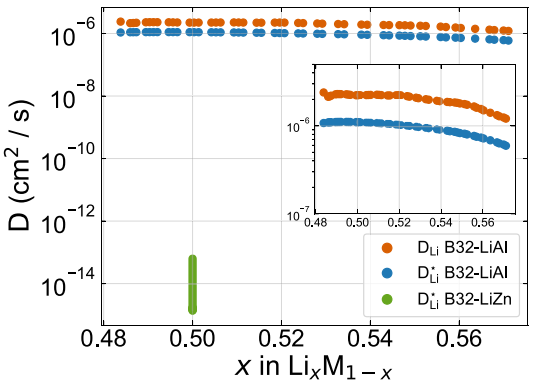

Figure 4. Calculated Li collective and tracer diffusion coefficients in B32 LiAl along with the Li tracer diffusion in B32 LiZn at 300 K as a function of composition. The B32 LiZn intermetallic is only stable in a very narrow composition window around the stoichiometric composition of x = 0.5 and its equilibrium vacancy concentration varies by 2 orders of magnitude over this narrow composition interval, leading to a widespread in the Li tracer diffusion coefficient. Since the predicted vacancy concentration is very low in B32 LiZn, analytical expressions for the tracer diffusion coefficient can be used.[56]

of each hop,[31,58] and thereby rigorously accounting for all the possible interactions between species that affect the trajectories of diffusing atoms. Figure 4 shows the calculated diffusion coefficients of lithium (blue dots), as a function of lithium composition in the B32 LiAl phase at 300 K. As is evident in the figure, a very high tracer diffusion coefficient of $\sim 10^{-6}$ cm^2/s is predicted for lithium when the composition is $x \approx 0.48$. This is consistent with the experimentally reported diffusion coefficients at room temperature by Tarczon et al.[23] The exceptionally high diffusion coefficient is a result of a very low migration barrier and a high concentration of vacancies on the Li sublattice. The vacancy concentration, while high, is not high enough to result in vacancy ordering,[59] as is evident in the sloping voltage profile in Figure 3a, or to lead to highly correlated diffusion as in layered and spinel intercalation compounds.[32,60] As the lithium content in the alloy increases, the tracer diffusion coefficient decreases by almost a factor of 2, in large part due to a similar decrease in the equilibrium vacancy concentration. Similar trends are observed for the collective diffusion coefficient[55,57] of Li (orange dots in Figure 4), which tracks the average displacement of the geometric center of all the diffusing Li.

In contrast to LiAl, the Li tracer diffusion coefficient in the LiZn zintl phase is very low, having values that range between 10^{-13} and 10^{-15} cm^2/s (green dots in Figure 4) within the voltage window in which LiZn is stable. The difference between the Li tracer diffusion coefficients of LiZn and LiAl is at least 7−9 orders of magnitude and is a result of a very low vacancy concentration in LiZn.

The stark difference in the equilibrium vacancy concentrations of LiAl and LiZn can be attributed to differences in their electronic structures. The metal sublattice of the B32 zintl phase has a diamond cubic crystal structure similar to the crystal structure of silicon (Figure 1a). While Zn is a transition metal with valence d orbitals, Al has a valence electron structure similar to Si, but is short one electron to fill all the bonding states. The addition of Li to a diamond crystal structure of Al to form B32 LiAl does not significantly alter the electronic structure of Al in the diamond crystal structure, with Li primarily donating electrons to the host and thereby filling bonding states (Figure 5a). Nevertheless, in contrast to diamond Si and diamond Al (electronic structure of B32 LiAl without Li is shown in Figure S4), the presence of Li in B32 LiAl eliminates the band gap that separates the bonding states from the antibonding states, resulting in a semimetal.[61] This is clearly observed in the band structure (Figure 5b) where a small overlap between valence and conduction bands is seen near the Fermi level.

The calculated electronic density of states plot for stoichiometric B32-LiAl, shown in Figure 5a, indicates that it is the overlap between the bonding and antibonding states that causes a preference for the formation of structural vacancies in B32-LiAl. In stoichiometric B32-LiAl, the Fermi level resides to the right of a cusp where the bonding and antibonding states meet, and a small fraction of antibonding states are filled. This is corroborated by a Crystal Orbital Hamiltonian Population (COHP) analysis (Figure S5), which shows the presence of antibonding states below the Fermi level of stoichiometric B32-LiAl. Furthermore, a closer look at the band structure near the Fermi level (Figure 5c) also indicates that some of the antibonding states belonging to the conduction band are filled near the high-symmetry k-point X, consistent with the previous reports by Asada et al.[63] However, upon the introduction of Li-vacancies, the fraction of antibonding states that are filled

https://doi.org/10.1021/acsenergylett.5c00266
ACS Energy Lett. 2025, 10, 1772−1778

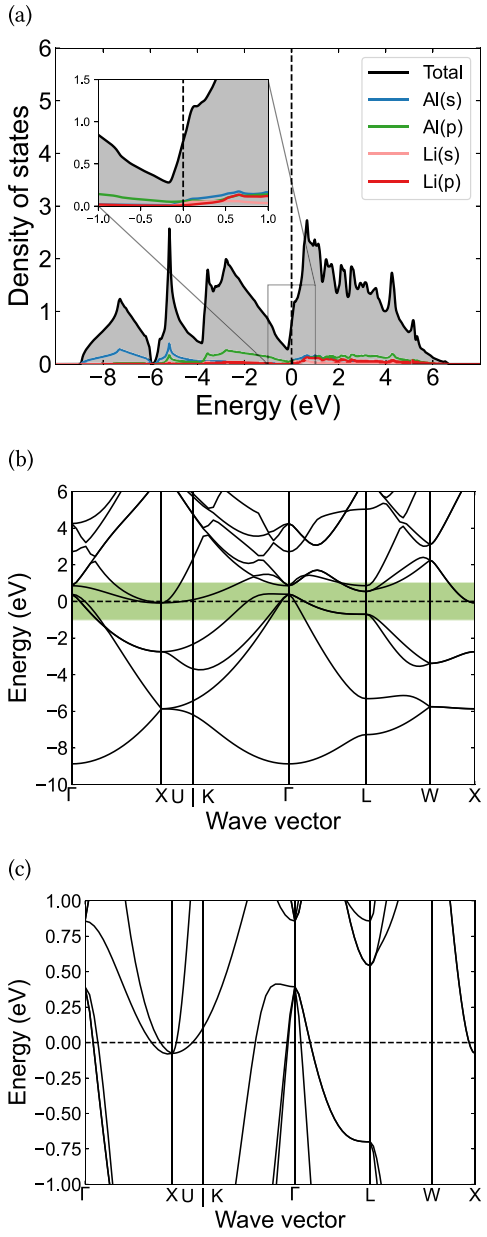

Figure 5. (a) Electronic density of states of B32 LiAl. The black dashed line denotes the Fermi level. The reported projected density of states is computed using the projector functions provided by the PAW[62] method and includes individual contributions from all the atoms in the unit cell. (b) Band structure of B32 LiAl along the high-symmetry Γ−X−U | K−Γ−L−W−X path in the reciprocal space. The green portion highlights the band structure near the Fermi level and is also shown in panel (c).

decreases since the compound now has fewer valence electrons. This is consistent with previous observations,[63,64] which also relate the stability of Li-vacancies to the electronic structure of B32-LiAl. A similar lowering of the Fermi level occurs upon the formation of Li-antisite defects on the Al-sublattice as this also reduces the total number of electrons of the compound, making Li-antisite defects favorable at higher Li compositions.

In anode-free batteries, electrochemically deposited Li will initially react with alloying additives to form either a solid solution or a series of intermetallics,[34] each stable within a specific voltage window. While the mechanisms with which these phases affect subsequent Li plating and stripping remain poorly understood, the role of Li diffusion within the intermetallic compounds has been hypothesized as playing an important role. The formed intermetallics may aid the nucleation of lithium metal to ensure a more uniform deposition. Alternatively, the formed intermetallics may serve as an interphase that wets the solid-electrolyte surface and thereby fosters a more uniform deposition of lithium metal on the opposite side of the interphase. In this scenario, diffusion through the intermetallic is crucial to enable lithium transport through the interphase followed by deposition and growth of lithium metal. However, very high diffusion coefficients may not always be desirable, as it can lead to hysteresis phenomena.[37,65] The successful identification of strategies to overcome dendrite and void formation during lithium plating and stripping in anode-free batteries will enable an almost 3-fold increase in energy densities of Li-ion batteries. The results of this study show that the Li diffusion coefficients within intermetallics span a wide range, offering battery designers tremendous flexibility in tailoring the transport properties of interphase layers in all-solid-state batteries.

■ ASSOCIATED CONTENT

Supporting Information

The Supporting Information is available free of charge at https://pubs.acs.org/doi/10.1021/acsenergylett.5c00266.

Density functional theory and Monte Carlo simulation details; tracer diffusion coefficients, correlation factors of lithium and vacancy in the LiAl zintl phase at 300 K; Haven ratio of the LiAl zintl phase at 300 K; Li−Zn voltage at 300 K; equilibrium vacancy concentration of LiZn zintl phase at 300 K; density of states of B32-LiAl with lithium taken out from the crystal structure; COHP analysis of B32-LiAl; density of states of B32-LiZn (PDF)

■ AUTHOR INFORMATION

Corresponding Author

Anton Van der Ven − *Materials Department, University of California Santa Barbara, Santa Barbara, California 93106, United States*; Email: avdv@ucsb.edu

Author

Sesha Sai Behara − *Materials Department, University of California Santa Barbara, Santa Barbara, California 93106, United States*; orcid.org/0000-0003-2144-4586

Complete contact information is available at: https://pubs.acs.org/10.1021/acsenergylett.5c00266

Notes

The authors declare no competing financial interest.

■ ACKNOWLEDGMENTS

S.S.B. and A.V.D.V. were supported by the National Science Foundation, under contract No. 2311370. Use was made of computational facilities purchased with funds from the National Science Foundation (CNS-1725797) and administered by the Center for Scientific Computing (CSC). The CSC is supported by the California NanoSystems Institute and the Materials Research Science and Engineering Center (MRSEC; NSF DMR No. 2308708) at UC Santa Barbara. We are also

grateful for the resources of the National Energy Research Scientific Computing Center (NERSC), a U.S. Department of Energy Office of Science User Facility located at Lawrence Berkeley National Laboratory, operated under Contract No. DE-AC02-05CH11231 using NERSC Award No. BES-ERCAP0026626. Research was also carried out at the Center for Functional Nanomaterials, Brookhaven National Laboratory, through the U.S. Department of Energy, Office of Basic Energy Sciences, contract DE-AC02-98CH10866, under Award No. CFN312109.

REFERENCES

(1) Janek, J.; Zeier, W. G. A solid future for battery development. *Nat. Energy* **2016**, *1*, 1−4.
(2) Wang, M. J.; Kazyak, E.; Dasgupta, N. P.; Sakamoto, J. Transitioning solid-state batteries from lab to market: Linking electro-chemo-mechanics with practical considerations. *Joule* **2021**, *5*, 1371−1390.
(3) Kasemchainan, J.; Zekoll, S.; Spencer Jolly, D.; Ning, Z.; Hartley, G. O.; Marrow, J.; Bruce, P. G. Critical stripping current leads to dendrite formation on plating in lithium anode solid electrolyte cells. *Nature materials* **2019**, *18*, 1105−1111.
(4) Krauskopf, T.; Hartmann, H.; Zeier, W. G.; Janek, J. Toward a fundamental understanding of the lithium metal anode in solid-state batteries—an electrochemo-mechanical study on the garnet-type solid electrolyte Li6. 25Al0. 25La3Zr2O12. *ACS Appl. Mater. Interfaces* **2019**, *11*, 14463−14477.
(5) Porz, L.; Swamy, T.; Sheldon, B. W.; Rettenwander, D.; Frömling, T.; Thaman, H. L.; Berendts, S.; Uecker, R.; Carter, W. C.; Chiang, Y.-M. Mechanism of lithium metal penetration through inorganic solid electrolytes. *Adv. Energy Mater.* **2017**, *7*, 1701003.
(6) Ning, Z.; Jolly, D. S.; Li, G.; De Meyere, R.; Pu, S. D.; Chen, Y.; Kasemchainan, J.; Ihli, J.; Gong, C.; Liu, B.; et al. Visualizing plating-induced cracking in lithium-anode solid-electrolyte cells. *Nature materials* **2021**, *20*, 1121−1129.
(7) Kazyak, E.; Garcia-Mendez, R.; LePage, W. S.; Sharafi, A.; Davis, A. L.; Sanchez, A. J.; Chen, K.-H.; Haslam, C.; Sakamoto, J.; Dasgupta, N. P. Li penetration in ceramic solid electrolytes: operando microscopy analysis of morphology, propagation, and reversibility. *Matter* **2020**, *2*, 1025−1048.
(8) Sandoval, S. E.; Haslam, C. G.; Vishnugopi, B. S.; Liao, D. W.; Yoon, J. S.; Park, S. H.; Wang, Y.; Mitlin, D.; Hatzell, K. B.; Siegel, D. J.; et al. Electro-chemo-mechanics of anode-free solid-state batteries. *Nat. Mater.* **2025**, 1−9.
(9) Liu, Y.; Wang, C.; Yoon, S. G.; Han, S. Y.; Lewis, J. A.; Prakash, D.; Klein, E. J.; Chen, T.; Kang, D. H.; Majumdar, D.; Gopalaswamy, R.; McDowell, M. T.; et al. Aluminum foil negative electrodes with multiphase microstructure for all-solid-state Li-ion batteries. *Nat. Commun.* **2023**, *14*, 3975.
(10) Cao, J.; Shi, Y.; Gao, A.; Du, G.; Dilxat, M.; Zhang, Y.; Cai, M.; Qian, G.; Lu, X.; Xie, F.; Sun, Y.; Lu, X.; et al. Hierarchical Li electrochemistry using alloy-type anode for high-energy-density Li metal batteries. *Nat. Commun.* **2024**, *15*, 1354.
(11) Lee, Y.-G.; Fujiki, S.; Jung, C.; Suzuki, N.; Yashiro, N.; Omoda, R.; Ko, D.-S.; Shiratsuchi, T.; Sugimoto, T.; Ryu, S.; et al. High-energy long-cycling all-solid-state lithium metal batteries enabled by silver−carbon composite anodes. *Nature Energy* **2020**, *5*, 299−308.
(12) Liang, X.; Pang, Q.; Kochetkov, I. R.; Sempere, M. S.; Huang, H.; Sun, X.; Nazar, L. F. A facile surface chemistry route to a stabilized lithium metal anode. *Nat. Energy* **2017**, *2*, 1−7.
(13) Yang, C.; Xie, H.; Ping, W.; Fu, K.; Liu, B.; Rao, J.; Dai, J.; Wang, C.; Pastel, G.; Hu, L. An electron/ion dual-conductive alloy framework for high-rate and high-capacity solid-state lithium-metal batteries. *Adv. Mater.* **2019**, *31*, 1804815.
(14) Choi, S. H.; Lee, S. J.; Yoo, D.-J.; Park, J. H.; Park, J.-H.; Ko, Y. N.; Park, J.; Sung, Y.-E.; Chung, S.-Y.; Kim, H.; Choi, J. W.; et al. Marginal magnesium doping for high-performance lithium metal batteries. *Adv. Energy Mater.* **2019**, *9*, 1902278.
(15) Kim, S.; Jung, C.; Kim, H.; Thomas-Alyea, K. E.; Yoon, G.; Kim, B.; Badding, M. E.; Song, Z.; Chang, J.; Kim, J.; Im, D.; Kang, K.; et al. The role of interlayer chemistry in Li-metal growth through a garnet-type solid electrolyte. *Adv. Energy Mater.* **2020**, *10*, 1903993.
(16) Krauskopf, T.; Mogwitz, B.; Rosenbach, C.; Zeier, W. G.; Janek, J. Diffusion limitation of lithium metal and Li−Mg alloy anodes on LLZO type solid electrolytes as a function of temperature and pressure. *Adv. Energy Mater.* **2019**, *9*, 1902568.
(17) Siniscalchi, M.; Liu, J.; Gibson, J. S.; Turrell, S. J.; Aspinall, J.; Weatherup, R. S.; Pasta, M.; Speller, S. C.; Grovenor, C. R. On the relative importance of Li bulk diffusivity and interface morphology in determining the stripped capacity of metallic anodes in solid-state batteries. *ACS Energy Letters* **2022**, *7*, 3593−3599.
(18) Wan, M.; Kang, S.; Wang, L.; Lee, H.-W.; Zheng, G. W.; Cui, Y.; Sun, Y. Mechanical rolling formation of interpenetrated lithium metal/lithium tin alloy foil for ultrahigh-rate battery anode. *Nat. Commun.* **2020**, *11*, 829.
(19) Jin, S.; Ye, Y.; Niu, Y.; Xu, Y.; Jin, H.; Wang, J.; Sun, Z.; Cao, A.; Wu, X.; Luo, Y.; et al. Solid−solution-based metal alloy phase for highly reversible lithium metal anode. *J. Am. Chem. Soc.* **2020**, *142*, 8818−8826.
(20) Hiratani, M.; Miyauchi, K.; Kudo, T. Effect of a lithium alloy layer inserted between a lithium anode and a solid electrolyte. *Solid State Ionics* **1988**, *28-30*, 1406−1410.
(21) Behara, S. S.; Van der Ven, A. Role of Short-Range Order on Diffusion Coefficients in the Li−Mg Alloy. *Chem. Mater.* **2024**, *36*, 11236−11245.
(22) Chen, S.; Tarczon, J. C.; Halperin, W.; Brittain, J. Li self-diffusion in pure and doped β-LiAl using pulsed-field gradient NMR. *J. Phys. Chem. Solids* **1985**, *46*, 895−904.
(23) Tarczon, J.; Halperin, W.; Chen, S.; Brittain, J. Vacancy-antistructure defect interaction diffusion in β-LiAl and β-LiIn. *Materials Science and Engineering: A* **1988**, *101*, 99−108.
(24) Wen, C. J.; Boukamp, B.; Huggins, R. A.; Weppner, W. Thermodynamic and mass transport properties of "LiAl". *J. Electrochem. Soc.* **1979**, *126*, 2258.
(25) Allnatt, A. R.; Lidiard, A. B. *Atomic Transport in Solids*; Cambridge University Press, 2003.
(26) Van der Ven, A.; Yu, H.-C.; Ceder, G.; Thornton, K. Vacancy mediated substitutional diffusion in binary crystalline solids. *Prog. Mater. Sci.* **2010**, *55*, 61−105.
(27) Xu, Q.; Van der Ven, A. First-principles investigation of migration barriers and point defect complexes in B2−NiAl. *Intermetallics* **2009**, *17*, 319−329.
(28) Xu, Q.; Van der Ven, A. Atomic transport in ordered compounds mediated by local disorder: Diffusion in B 2-Ni x Al 1- x. *Phys. Rev. B: Condensed Matter Mater. Phys.* **2010**, *81*, No. 064303.
(29) Thomas, J.; Behara, S. S.; Van der Ven, A. Thermodynamic and Kinetic Properties of the Lithium−Silver System. *Chem. Mater.* **2024**, *36*, 8936−8948.
(30) Van der Ven, A.; Ceder, G. First principles calculation of the interdiffusion coefficient in binary alloys. *Physical review letters* **2005**, *94*, No. 045901.
(31) Goiri, J. G.; Kolli, S. K.; Van der Ven, A. Role of short-and long-range ordering on diffusion in Ni-Al alloys. *Physical Review Materials* **2019**, *3*, No. 093402.
(32) Van der Ven, A.; Bhattacharya, J.; Belak, A. A. Understanding Li diffusion in Li-intercalation compounds. *Accounts of chemical research* **2013**, *46*, 1216−1225.
(33) Raju Natarajan, A.; Van der Ven, A. Toward an understanding of deformation mechanisms in metallic lithium and sodium from first-principles. *Chem. Mater.* **2019**, *31*, 8222−8229.
(34) Behara, S. S.; Thomas, J.; Van der Ven, A. Fundamental Thermodynamic, Kinetic, and Mechanical Properties of Lithium and Its Alloys. *Chem. Mater.* **2024**, *36*, 7370−7387.
(35) Schott, V.; Fähnle, M.; Madden, P. Theory of self-diffusion in alkali metals: I. Results for monovacancies in Li, Na, and K. *J. Phys.: Condens. Matter* **2000**, *12*, 1171.

https://doi.org/10.1021/acsenergylett.5c00266
ACS Energy Lett. 2025, 10, 1772−1778

(36) Frank, W.; Breier, U.; Elsässer, C.; Fähnle, M. First-principles calculations of absolute concentrations and self-diffusion constants of vacancies in lithium. *Physical review letters* **1996**, *77*, 518.
(37) Chang, D.; Huo, H.; Johnston, K. E.; Ménétrier, M.; Monconduit, L.; Grey, C. P.; Van der Ven, A. Elucidating the origins of phase transformation hysteresis during electrochemical cycling of Li−Sb electrodes. *Journal of Materials Chemistry A* **2015**, *3*, 18928−18943.
(38) Hansel, C.; Singh, B.; Kiwic, D.; Canepa, P.; Kundu, D. Favorable interfacial chemomechanics enables stable cycling of high-Li-content Li−In/Sn anodes in sulfide electrolyte-based solid-state batteries. *Chem. Mater.* **2021**, *33*, 6029−6040.
(39) Wang, Y.; Richards, W. D.; Ong, S. P.; Miara, L. J.; Kim, J. C.; Mo, Y.; Ceder, G. Design principles for solid-state lithium superionic conductors. *Nature materials* **2015**, *14*, 1026−1031.
(40) Emly, A.; Kioupakis, E.; Van der Ven, A. Phase stability and transport mechanisms in antiperovskite Li3OCl and Li3OBr superionic conductors. *Chem. Mater.* **2013**, *25*, 4663−4670.
(41) He, X.; Zhu, Y.; Mo, Y. Origin of fast ion diffusion in super-ionic conductors. *Nat. Commun.* **2017**, *8*, 15893.
(42) Kresse, G.; Hafner, J. Ab initio molecular dynamics for liquid metals. *Phys. Rev. B* **1993**, *47*, 558.
(43) Kresse, G.; Furthmüller, J. Efficiency of ab-initio total energy calculations for metals and semiconductors using a plane-wave basis set. *Computational materials science* **1996**, *6*, 15−50.
(44) Kresse, G.; Furthmüller, J. Efficient iterative schemes for ab initio total-energy calculations using a plane-wave basis set. *Phys. Rev. B* **1996**, *54*, 11169.
(45) Sheppard, D.; Terrell, R.; Henkelman, G. Optimization methods for finding minimum energy paths. *J. Chem. Phys.* **2008**, *128*, 134106.
(46) Henkelman, G.; Uberuaga, B. P.; Jónsson, H. A climbing image nudged elastic band method for finding saddle points and minimum energy paths. *J. Chem. Phys.* **2000**, *113*, 9901−9904.
(47) Henkelman, G.; Jónsson, H. Improved tangent estimate in the nudged elastic band method for finding minimum energy paths and saddle points. *J. Chem. Phys.* **2000**, *113*, 9978−9985.
(48) Mantina, M.; Wang, Y.; Arroyave, R.; Chen, L.; Liu, Z.-K.; Wolverton, C. First-principles calculation of self-diffusion coefficients. *Physical review letters* **2008**, *100*, 215901.
(49) Wu, H.; Mayeshiba, T.; Morgan, D. High-throughput ab-initio dilute solute diffusion database. *Sci. Data* **2016**, *3*, 1−11.
(50) Puchala, B.; Thomas, J. C.; Natarajan, A. R.; Goiri, J. G.; Behara, S. S.; Kaufman, J. L.; Van der Ven, A. CASM—A software package for first-principles based study of multicomponent crystalline solids. *Comput. Mater. Sci.* **2023**, *217*, 111897.
(51) Pelton, A. The Li-Zn (lithium-zinc) system. *Journal of phase equilibria* **1991**, *12*, 42−45.
(52) Belak, A. A.; Van der Ven, A. Effect of disorder on the dilute equilibrium vacancy concentrations of multicomponent crystalline solids. *Phys. Rev. B* **2015**, *91*, 224109.
(53) Jacucci, G.; Taylor, R. The calculation of vacancy formation energies in the alkali metals Li, Na and K. *Journal of Physics F: Metal Physics* **1979**, *9*, 1489.
(54) Hwa, Y.; Sung, J. H.; Wang, B.; Park, C.-M.; Sohn, H.-J. Nanostructured Zn-based composite anodes for rechargeable Li-ion batteries. *J. Mater. Chem.* **2012**, *22*, 12767−12773.
(55) Van der Ven, A.; Deng, Z.; Banerjee, S.; Ong, S. P. Rechargeable alkali-ion battery materials: theory and computation. *Chem. Rev.* **2020**, *120*, 6977−7019.
(56) Balluffi, R. W.; Allen, S. M.; Carter, W. C. *Kinetics of Materials*; John Wiley & Sons, 2005.
(57) Puchala, B.; Thomas, J. C.; Van der Ven, A. CASM Monte Carlo: Calculations of the thermodynamic and kinetic properties of complex multicomponent crystals. arXiv preprint arXiv:2309.11761, 21 September 2023; https://arxiv.org/abs/2309.11761, Accessed March 11, 2025.
(58) Van der Ven, A.; Thomas, J. C.; Puchala, B.; Natarajan, A. R. First-principles statistical mechanics of multicomponent crystals. *Annu. Rev. Mater. Res.* **2018**, *48*, 27−55.
(59) Goiri, J. G.; Van der Ven, A. Phase and structural stability in Ni-Al systems from first principles. *Phys. Rev. B* **2016**, *94*, No. 094111.
(60) Kolli, S. K.; Van der Ven, A. Elucidating the factors that cause cation diffusion shutdown in spinel-based electrodes. *Chem. Mater.* **2021**, *33*, 6421−6432.
(61) Zunger, A. First-principles theoretical study on the electronic properties of the B 32 intermetallic compound LiAl. *Phys. Rev. B* **1978**, *17*, 2582.
(62) Blöchl, P. E. Projector augmented-wave method. *Phys. Rev. B* **1994**, *50*, 17953.
(63) Asada, T.; Jarlborg, T.; Freeman, A. J. Self-consistent electronic structure of the intermetallic compound LiA1. *Phys. Rev. B* **1981**, *24*, 510.
(64) Kishio, K.; Brittain, J. Defect structure of β-LiAl. *J. Phys. Chem. Solids* **1979**, *40*, 933−940.
(65) Van der Ven, A.; See, K. A.; Pilon, L. Hysteresis in electrochemical systems. *Battery Energy* **2022**, *1*, 20210017.

https://doi.org/10.1021/acsenergylett.5c00266
ACS Energy Lett. 2025, 10, 1772−1778